Inorg. Chem. **2006**, *45*, 4695–4705

Inorganic Chemistry

Article

Spectroscopic, Magnetochemical, and Crystallographic Study of Cesium Iron Phosphate Hexahydrate: Characterization of the Electronic Structure of the Iron(II) Hexa-aqua Cation in a Quasicubic Environment

Graham Carver,[†] Christopher Dobe,[†] Thomas B. Jensen,[†] Philip L. W. Tregenna-Piggott,*,[†,‡] Stefan Janssen,[‡] Eckhard Bill,[§] Garry J. McIntyre,[||] and Anne-Laure Barra[⊥]

Department of Chemistry and Biochemistry, University of Bern, Freiestrasse 3, 3012 Bern, Switzerland, Laboratory for Neutron Scattering, ETH Zürich and Paul-Scherrer Institute, CH-5232 Villigen PSI, Switzerland, Max-Planck-Institut für Bioanorganische Chemie, Stiftstrasse 34-36, D-45470 Mülheim an der Ruhr, Germany, Institut Laue-Langevin, BP156, 38042 Grenoble Cedex 9, France, and High Magnetic Field Laboratory, CNRS/MPI, B.P. 166, 38042 Grenoble, France

Received February 2, 2006

Spectroscopic, magnetochemical, and crystallographic data are presented for $CsFe(H_2O)_6PO_4$, a member of a little-known isomorphous series of salts that facilitates the study of hexa-aqua ions in a quasicubic environment. Above 120 K, the deviations from cubic symmetry are minimal, as shown by the first example of an iron(II) Mössbauer spectrum that exhibits no measurable quadrupole splitting. Two crystallographically distinct $[Fe(OH_2)_6]^{2+}$ complexes are identified from inelastic neutron-scattering (INS) experiments conducted between 2 and 15 K. The data are modeled with the ligand-field Hamiltonian, $\hat{H} = \lambda\hat{L}\hat{S} + \beta B(k\hat{L} + 2\hat{S}) + \Delta_{tet}\{\hat{L}_z^2 - (1/3)L(L+1)\} + \Delta_{rhom}\{\hat{L}_x^2 - \hat{L}_y^2\}$, operating in the ground-term $^5T_{2g}$ (O_h) basis. An excellent reproduction of INS, Mössbauer, HF-EPR, and magnetochemical data are obtained in the 2 and 15 K temperature regimes with the following parameters: $\lambda =$ –80 cm^{-1}; $k = 0.8$; site A $\Delta_{tet} = 183$ cm^{-1}, $\Delta_{rhom} = 19$ cm^{-1}; site B $\Delta_{tet} = 181$ cm^{-1}, $\Delta_{rhom} = 12$ cm^{-1}. The corresponding zero-field-splitting (ZFS) parameters of the conventional $S = 2$ spin Hamiltonian are as follows: site A $D = 12.02$ cm^{-1}, $E = 2.123$ cm^{-1}; site B $D = 12.15$ cm^{-1}, $E = 1.37$ cm^{-1}. A theoretical analysis of the variation of the energies of the low-lying states with respect to displacements along selected normal coordinates of the $[Fe(OH_2)_6]^{2+}$, shows the zero-field splitting to be extremely sensitive to small structural perturbations of the complex. The expressions derived are discussed in the context of spin-Hamiltonian parameters reported for the $[Fe(OH_2)_6]^{2+}$ cation in different crystalline environments.

1. Introduction

Aqua ions are the most fundamental species that exist in aqueous solution. The study of their structure, bonding, and reactivity is necessary not only for an understanding of solution chemistry but also for a comprehension of the physical and chemical properties of the elements themselves. Many experimental studies have focused on the solid state, where the aqua ions are held rigidly in a crystalline environment, thus facilitating their characterization; the drawback being the difficulty in assessing the role that the host plays in dictating their electronic and molecular structures.[1−7] Theoretical predictions of the most stable conformations of aqua

---

* To whom correspondence should be addressed. E-mail: philip.tregenna@psi.ch.

[†] University of Bern.

[‡] ETH Zürich and Paul-Scherrer Institute.

[§] Max-Planck-Institut für Bioanorganische Chemie.

[||] Institut Laue-Langevin.

[⊥] High Magnetic Field Laboratory.

(1) Simmons, C. J.; Hitchman, M. A.; Stratemeier, H.; Schultz, A. J. *J. Am. Chem. Soc.* **1993**, *115*, 11304.

(2) Best S. P.; Forsyth, J. B. *J. Chem. Soc., Dalton Trans.* **1991**, 1721.

(3) Cotton, F. A.; Fair, C. K.; Lewis, G. E.; Mott, G.; Moss, F. K.; Schultz, A. J.; Williams, M. J. *J. Am. Chem. Soc.* **1984**, *106*, 5319.

(4) Bussière, G.; Beaulac, R.; Cardinal-David, B.; Reber, C. *Coord. Chem. Rev.* **2001**, *219−221*, 509−543.

(5) Tregenna-Piggott, P. L. W.; Andres, H. P.; McIntyre, G. J.; Best, S. P.; Wilson, C. C.; Cowan, J. A. *Inorg. Chem.* **2003**, *42*, 1350.

(6) Ptasiewiczbak, H.; Olovsson, I.; McIntyre, G. J. *Acta Crystallogr. B* **1997**, *53*, 325−336.

(7) Telser, J.; van Slageren, J.; Vongtragool, S.; Dressel, M.; Reiff, W. M.; Zvyagin, S. A.; Ozarowski, A.; Krzystek, J. *Magn. Reson. Chem.* **2005**, *43*, 130−139.

10.1021/ic0601889 CCC: $33.50

ions are often difficult to verify in low-symmetry crystalline hydrates, as the distortion away from a high-symmetry structure is to some degree a result of steric hydrogen-bonding constraints.[5,8−11] The modeling of magnetochemical,[12,13] spectroscopic,[7] and polarized neutron-diffraction[14] data is often confounded by the lack of symmetry for the site on which the metal cation resides, leading to ambiguity in the definition of the bonding parameters. These complications are alleviated somewhat in crystal systems where the aqua ions lie on sites of axial symmetry, a prime example being the alums where anomalies in the structural chemistry can be confidently related to the detailed electronic structure of the complex.[2,5,15−18]

An ideal crystal system in which to study the structure and bonding of aqua ions is one that has a cubic site for the metal ion. The family of salts $CsM^{II}(H_2O)_6XO_4$, where M^{II} is a divalent cation and X = As, P, constitutes such a model system, promising to become a favorite among symmetry-mongers. Crystallographic studies undertaken 50 years ago demonstrated that the majority of the salts crystallize in a face-centered cubic lattice, in which the bivalent hexa-aqua ion resides on a site of T_d symmetry.[19] The $CsMg(H_2O)_6AsO_4$ salt is unusual in that single crystals can be readily prepared, yielding a more precise crystallographic characterization.[19(b)] Since then, the system has been forgotten, as we are unaware of any measurements to elucidate the electronic structure of these salts. This work presents a detailed experimental study of $CsFe(H_2O)_6PO_4$. The high site symmetry provides an excellent opportunity to study Fe(II)−water bonding interactions, and iron(II) complexes may be probed by a comprehensive armory of modern spectroscopic techniques. In view of its importance to a number of biological and environmental chemical processes, the $[Fe(OH_2)_6]^{2+}$ cation has been studied extensively, but discrepancies in the definition of the bonding parameters have remained.[7,11−14,20,21]

Mössbauer, high-field EPR (HFEPR), inelastic neutron scattering (INS), and magnetochemical measurements are presented, providing a rigorous definition of the electronic structure of the $[Fe(OH_2)_6]^{2+}$ cation in the $CsFe(H_2O)_6PO_4$ host, and they may be satisfactorily modeled using a ligand-field Hamiltonian operating in the ground term $^5T_{2g}$ (O_h) basis. The results are interpreted in conjunction with angular overlap model (AOM) calculations, from which expressions relating the energies of the low-lying states of a hexacoordinate Fe(II) cation to distortions along selected symmetrized coordinates, are derived.

2. Experimental Section

2.1. Synthesis. Difficulties were experienced in the preparation of $CsFe(H_2O)_6PO_4$ as originally described.[19] The following method was found to be reliable in yielding the desired product. All procedures were carried out with the rigorous exclusion of oxygen using standard Schlenk techniques under nitrogen gas. $CsNO_3$ (12 g) was dissolved in 100 mL of an aqueous solution containing 1.35 mL of H_3PO_4 (85%) and three drops of phenolphthalein solution. The subsequent dissolution of $FeSO_4{\cdot}7H_2O$ (5 g) gave a light green solution. The apparatus was immersed in an ice−water bath and cooled to ∼5 °C. A pale green precipitate formed upon dropwise addition of an ammonia solution (1%). The fine material was filtered on a G4 frit once the color of the solution became pale pink, indicating a pH of ∼10. The product was washed with acetone, dried under a flow of nitrogen gas, and finally placed under vacuum. Attempts to prepare samples suitable for single-crystal diffraction measurements have to date been unsuccessful. This is frustrating, as large single crystals of $CsNi(H_2O)_6PO_4$ and $CsMg(H_2O)_6AsO_4$ can be readily prepared. Cesium iron phosphate hexahydrate is extremely prone to oxidation when moist. $CsFe(D_2O)_6PO_4$ was prepared following the same procedure, using deuterated chemicals obtained from Armar AG.

2.2. Powder Diffraction Measurements. Powder X-ray diffraction (PXRD) was performed on a STOE STADI P diffractometer in transmission mode, using Cu Kα radiation from a curved Ge(111) monochromator and a linear position-sensitive detector. The sample was sealed in a 0.3 mm diameter glass capillary. Five diffraction patterns were obtained in the range of $2\theta = 10-105°$ at 296 K, compared for decomposition and intensity changes, and then summed. Data above 93° were discarded because of the partial obscuration of the detector.

Neutron powder-diffraction measurements were carried out on the powder diffractometer D1a at the Institut Laue-Langevin, Grenoble, France. A wavelength of 1.9106 Å was obtained from a Ge(115) crystal monochromator. A 10 mm vanadium cylinder was filled in an argon glovebox with a fully deuterated sample of $CsFe(D_2O)_6PO_4$ and mounted on the coldfinger of a displex cryostat. Data were collected at 50 and 7 K in the 2θ range of 10−157° in 0.05° steps.

Rietveld refinements were performed with the program FULLPROF[22] on both the X-ray-diffraction and neutron-diffraction data sets. The background was defined by a refinable set of points with linear interpolation, and the peak profiles were generated with a pseudo-Voigt function.

2.3. Magnetic Measurements. Magnetic susceptibility measurements of a powdered sample of $CsFe(D_2O)_6PO_4$ were conducted on a Quantum-Design MPMS-XL SQUID magnetometer at the University of Bern. Samples (10−20 mg) were sealed in gelatine capsules under dry nitrogen; measurements were obtained using a field strength of 0.1 T at temperatures between 1.8 and 300 K.

2.4. Inelastic Neutron Scattering. INS measurements were carried out on the time-of-flight spectrometer FOCUS at the Paul

---

(8) Kallies, B.; Meier, R. *Inorg. Chem.* **2001**, *40*, 3101.
(9) Åkesson, R.; Pettersson, L. G. M.; Sandström, M.; Wahlgren, U. *J. Am. Chem. Soc.* **1994**, *116*, 8691.
(10) Benmelouka, M.; Messaoudi, S.; Furet, E.; Gautier, R.; Le Fur, E.; Pivan, J.-Y. *J. Phys. Chem. A* **2003**, *107*, 4122−4129.
(11) Jarzeücki, A. A.; Anbar, A. D.; Spiro, T. G. *J. Phys. Chem. A* **2004**, *108*, 2726−2732.
(12) Figgis, B. N.; Lewis, J.; Mabbs, F. E.; Webb, G. A. *J. Chem. Soc. A* **1967**, 442.
(13) Gerloch, M.; Lewis, L.; Phillips, G. G.; Quested, P. N. *J. Chem. Soc. A* **1970**, 1941−1955.
(14) Figgis, B. N.; Forsyth, J. B.; Kucharski, E. S.; Reynolds, P. A.; Tasset, F. *Proc. R. Soc. London A* **1990**, *428*, 113−127.
(15) Tregenna-Piggott, P. L. W.; Best, S. P.; O'Brien, M. C. M.; Knight, K. S.; Forsyth, J. B.; Pilbrow, J. R. *J. Am. Chem. Soc.* **1997**, *119*, 3324.
(16) Tregenna-Piggott, P. L. W.; Best, S. P.; Güdel, H. U.; Weihe, H.; Wilson, C. C. *Sol. State Chem.* **1999**, *145*, 460.
(17) Tregenna-Piggott, P. L. W.; Güdel, H.-U. *Inorg. Chem.* **2001**, *40*, 5497.
(18) Beattie, J. K.; Best, S. P.; Del Favero, P.; Skelton, B. W.; Sobolev, A. N.; White, A. H. *J. Chem. Soc., Dalton Trans.* **1996**, 1481.
(19) Ferrari, A.; Cavalca, L.; Nardelli, M. *Gazz. Chim. Ital.* **1955**, *85*, 169−174. (b) Ferrari, A.; Tani, M. E.; Bonati, R. *Gazz. Chim. Ital.* **1956**, *86*, 1026−1030.
(20) Svare, I.; Otnes, K. *Physica B* **1983**, *120*, 159−162.
(21) Champion, P. M.; Sievers, A. J. *J. Chem. Phys.* **1977**, *66*, 1819.
(22) Rodriguez-Carvajal, J. *FULLPROF*, version 2.00; Institut Laue-Langevin: Grenoble, France, 2001.

Scherrer Institute, Villigen, Switzerland.[23] Approximately 5 g of a powdered, deuterated sample were loaded into a standard 10 × 50 mm aluminum cylinder under a He atmosphere. For measurements on the protonated material, approximately 3 g of sample were loaded into a 1 × 50 × 30 mm^3 aluminum flat-plate cell and oriented 45° to the incident neutron beam. Thin plate cells assist in minimizing multiple scattering. Data were collected between 1.5 and 40 K, utilizing a standard Orange ILL cryostat, and at wavelengths of 5.30, 4.75, and 2.70 Å, affording energy-transfer windows extending to 15, 25, and 75 cm^{-1}, respectively, on the neutron energy-loss side of the spectrum. Inelastic time focusing was employed at an energy transfer of 0 cm^{-1} for greatest resolution at the elastic-peak position.

2.5. EPR. High-field multifrequency EPR (HFEPR) measurements were carried out using the apparatus at the Grenoble High Magnetic Field Laboratory described in detail previously.[24] Samples were loaded to a depth of 10 mm in 4 mm o.d. quartz EPR tubes and sealed under a He atmosphere. Spectra were recorded employing excitation frequencies ranging from 95 to 475 GHz in conjunction with a static field ranging from 0 to 12 T at temperatures between 5 and 20 K.

2.6. Mössbauer Spectroscopy. Mössbauer spectra were recorded at the Max Planck Institut für Bioanorganische Chemie, Mülheim an der Ruhr, Germany, using an apparatus described previously.[25] Spectra were recorded in zero field from 200 to 4.2 K. Spectra were then recorded at 4.2 K in an applied magnetic field ranging from 0 to 7 T.

3. Ligand-Field Hamiltonian

The spectroscopic and magnetochemical data were interpreted with a ligand-field Hamiltonian, operating in the $^5T_{2g}$ (O_h) electronic basis, having the form

$$\hat{H} = \lambda\hat{L}\cdot\hat{S} + \beta B(k\hat{L} + 2\hat{S}) + \Delta_{\mathrm{tet}}\{\hat{L}_z^{\,2} - (1/3)L(L+1)\} + \Delta_{\mathrm{rhom}}\{\hat{L}_x^{\,2} - \hat{L}_y^{\,2}\} \quad (1)$$

All the data could be interpreted very satisfactorily using eq 1, with the spin−orbit-coupling constant, λ, orbital-reduction factor, k, and tetragonal and rhombic ligand-field parameters, Δ_{tet} and Δ_{rhom}, respectively, as variables. The inclusion of more basis functions and additional operators was not warranted as transitions were observed only between pairs of the three lowest-lying states.

The effective magnetic moment was calculated according to the procedure outlined in Supporting Information. EPR spectra were calculated by transforming the Zeeman matrices into the ligand-field eigenbasis and then calculating the resonance positions and intensities using the program SIM,[26] written by the celebrated Faroese chemist Høgni Weihe. INS spectra were also calculated directly from the energies and wave functions of the ligand-field Hamiltonian, as described previously.[27]

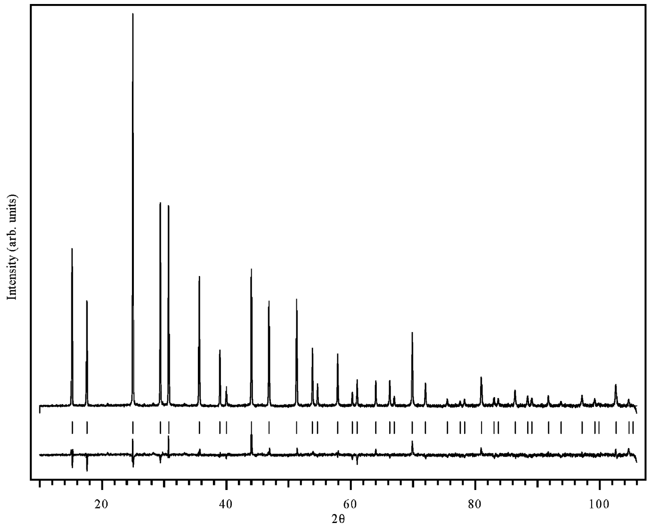

Figure 1. X-ray powder diffraction pattern of $CsFe(H_2O)_6PO_4$ recorded at 296 K. Bragg peak positions and the difference-pattern are indicated at the bottom of the figure.

The advantage of modeling the data directly with the ligand-field Hamiltonian, is the general applicability of the approach over the whole experimental temperature range, for an arbitrary set of parameters. When the strengths of the low-symmetry ligand fields are small compared to the spin−orbit coupling, an $S = 1$ spin Hamiltonian is appropriate to describe the magnetic properties of the perturbed $J = 1$ ground state at low magnetic fields. On the other hand, when the axial ligand field results in a ^5A_g ground term and the strength of this field is large compared to spin−orbit coupling, an $S = 2$ spin Hamiltonian can be employed to model the low-temperature data. For the system under consideration, the splitting of the $^5T_{2g}$ (O_h) ground term in the low-temperature regime, due to the ligand-field terms 3 and 4 in eq 1, is comparable to that of spin−orbit coupling. Nevertheless, for the purpose of relating the experimental data to the AOM calculations presented in section 5, the zero-field-splitting parameters of the $S = 1$ spin-Hamiltonian parameters are reported. Furthermore, so that this work can be readily related to other spectroscopic studies of Fe(II) complexes, the $S = 2$ spin-Hamiltonian parameters are also reported. We emphasize that while there is a 1:1 correspondence between the zero-field energies of the three lowest levels calculated from the ligand-field Hamiltonian and those calculated from the $S = 1$ and 2 spin Hamiltonians, the two highest eigenstates resulting from the $S = 2$ spin Hamiltonian have no relevance, as these states are not experimentally observed.

4. Results and Discussion

4.1. High-Temperature Phase, 120−298 K. A Rietveld refinement was performed on the 296 K powder X-ray diffraction pattern using the single-crystal neutron fractional coordinates of $CsNi(H_2O)_6PO_4$ as a starting point,[28] with all non-hydrogen atoms refined with anisotropic thermal parameters. The pattern, shown in Figure 1, refined well in

---

(23) Mesot, J.; Janssen, S.; Holitzner, L.; Hempelmann, R. *J. Neutron Res.* **1996**, *3*, 293.

(24) Muller, F.; Hopkins, A.; Coron, N.; Grynberg, M.; Brunel, L. C.; Martinez, G. *Rev. Sci. Instrum.* **1989**, *60*, 3681. (b) Barra, A. L.; Brunel, L. C.; Robert, J. B. *Chem. Phys. Lett.* **1990**, *165*, 107.

(25) Meyer, K.; Bill, E.; Mienert, B.; Weyhermüller, T.; Wieghardt, K. *J. Am. Chem. Soc.* **1999**, *121*, 4859−4876.

(26) Glerup, J.; Weihe, H. *Acta Chem. Scand.* **1991**, 444.

(27) Carver, G.; Tregenna-Piggott, P. L. W.; Barra, A.-L.; Neels, A.; Stride, J. A. *Inorg. Chem.* **2003**, *42*, 5771.

(28) Buergi, H.-B.; Carver, G.; Dobe, C.; Hauser, J.; McIntyre, G. J.; Tregenna-Piggott, P. L. W. Unpublished work.

Table 1. Crystal Data and Rietveld Structure Refinement for Powder Diffraction Data of $CsFe(H_2O)_6PO_4$

	x-ray	neutron
formula	$CsFe(H_2O)_6PO_4$	$CsFe(D_2O)_6PO_4$
fw	391.83 g/mol	403.83 g/mol
refinement method	Rietveld	Rietveld
wavelength	1.54060 Å	1.9105 Å
geometry	transmission	transmission
cryst syst	cubic	cubic
space group	$F\bar{4}3m$	$F\bar{4}3m$
Z	4	4
2θ range	10−93° (106°)	2−157.45°
step size	0.01°	0.05°
obsd reflns	39	48
no. of refined background points	9	8
no. of structural params	11	17
no. of profile params	8	8
total no. of refined params	28	33
no. of excluded regions		26

temp	296 K	50 K	7 K
unit cell	$a = 10.06024(5)$ Å	$a = 10.02420(9)$ Å	$a = 10.0189(1)$ Å
vol	1018.18(1) Å^3	1007.28(2) Å^3	1005.69(2) Å^3
Bragg R factor	4.71	3.25	5.80
R factors (including all nonexcluded points, not corrected for background)	$R_p = 1.33$ $R_{wp} = 1.81$ $R_{exp} = 1.25$ $\chi^2 = 2.09$	$R_p = 5.66$ $R_{wp} = 7.49$ $R_{exp} = 4.32$ $\chi^2 = 3.00$	$R_p = 7.10$ $R_{wp} = 13.5$ $R_{exp} = 2.47$ $\chi^2 = 30.0$

Table 2. Selected Bond Lengths (Å) and Angles (deg)

	x-ray 296 K	neutron 50 K	neutron 7 K
Fe−O(1)	2.141(3)	2.128(4)	2.123(5)
O(1)−O(2)	2.615(2)	2.618(4)	2.618(5)
O(1)−D		0.968(3)	0.973(4)
P−O(2)	1.561(1)	1.532(2)	1.531(3)
O(1)−D−O(2)		175.4(2)	172.47(5)

the space group $F\bar{4}3m$ to a final Bragg R factor of 4.71%. Details of the refinement are given in Table 1, and selected bond lengths are listed in Table 2. The Fe−O bond length of 2.141(3) Å is consistent with that found in other salts containing the $[Fe(OH_2)_6]^{2+}$ cation,[29,30] and the P−O bond length is consisent with that in the phosphate moiety of the Ni analogue.[28]

The position of the unique H atom could not be determined from these X-ray diffraction data, but the T_d site symmetry, on which the Fe(II) cation is located, largely dictates the stereochemistry of the $[Fe(OH_2)_6]^{2+}$ cation, which is illustrated in Figure 2. The mode of water coordination is trigonal planar with the plane of the unique water molecule rotated about the metal−oxygen bond vector by +45° with respect to the octahedral FeO_6 framework. The only degrees of freedom are the O−H bond lengths and the H−O−H bond angles. The projection shown in Figure 2 below was constructed assuming linear hydrogen bonds and an O−H bond length of 0.977 Å, corresponding to the average O−D bond length previously determined for the $(ND_4)_2Fe(D_2O)_6(SO_4)_2$ Tutton's salt.[30]

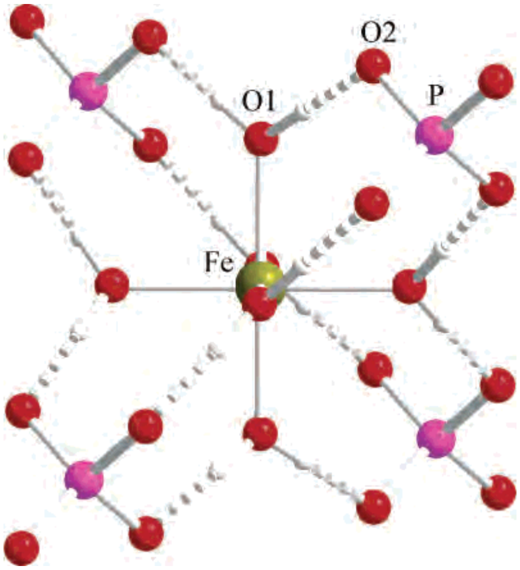

Figure 2. Coordination geometry about the Fe(II) cation in $CsFe(OH_2)_6PO_4$ constructed from a Rietveld refinement of the 296 K powder X-ray diffraction data.

Figure 3 displays Mössbauer spectra for $CsFe(H_2O)_6PO_4$ between 4.2 and 200 K, recorded in zero applied field.

In the 120−298 K temperature regime, the Mössbauer spectra exhibit a peak at $\delta \approx 1.3$ mm s^{-1}, with a quadrupole splitting of less than 0.073 mm s^{-1}. To our knowledge, this is the first example of a high-spin iron(II) complex with a negligible electric-field gradient at the ^{57}Fe nucleus, indicating that, in this temperature range the t_{2g} orbitals are virtually degenerate on the Mössbauer time scale (∼10^{-7} s).

Figure 4 shows the variation of μ_{eff} with temperature; the values were derived from the magnetization measurements

---

(29) Montgomery, H.; Chastain, R. V.; Natt, J. J.; Witkowska, A. M.; Lingafelter, E. C. *Acta Crystallogr.* **1967**, *22*, 775.

(30) Figgis, B. N.; Kucharski, E. S.; Reynolds, P. A.; Tasset, F. *Acta Crystallogr. C* **1989**, *45*, 942.

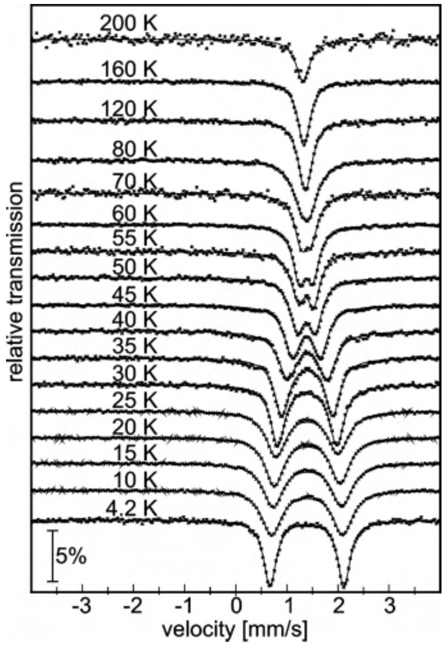

Figure 3. Zero-field Mössbauer spectra of $CsFe(H_2O)_6PO_4$ as a function of temperature. The solid lines are fits to a double Lorentzian function. The experimental spectra were corrected for a weak (2−5%) contribution from a ferric contaminant by subtraction of a Lorentzian doublet centered on $\delta \approx 0.3$ mm s^{-1}.

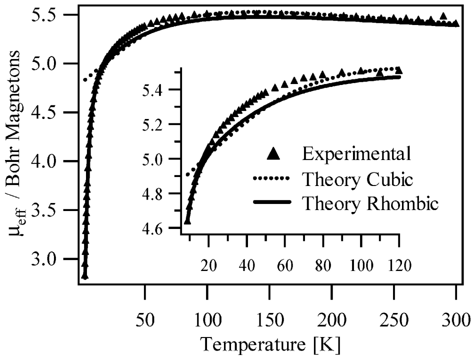

Figure 4. Variation of μ_{eff} with temperature for $CsFe(H_2O)_6PO_4$. Overlaid are theoretical curves calculated with $\lambda = -80$ cm^{-1} and $k = 0.8$. For the "Theory Cubic" curve, $\Delta_{tet} = \Delta_{rhom} = 0$. The "Theory Rhombic" curve represents the average value of μ_{eff} obtained from two calculations performed with the following parameters: calcd A $\Delta_{tet} = 183$ cm^{-1}, $\Delta_{rhom} = 19$ cm^{-1}; calcd B $\Delta_{tet} = 181$ cm^{-1}, $\Delta_{rhom} = 12$ cm^{-1}.

on powder samples of $CsFe(D_2O)_6PO_4$ from 2 to 296 K. A total of three samples was measured, with little variation in the molar susceptibility derived from each sample. The experimental data points, depicted by triangles, represent the average of the three measurements. The data are tabulated in Supporting Information. The room-temperature value of 5.38 μ_B is typical for an octahedrally coordinated high-spin Fe(II) complex,[31] with the moment increasing steadily upon cooling from 298 to 120 K.

The broken line on Figure 4 was calculated with $\lambda = -80$ cm^{-1}, $k = 0.8$, and all low-symmetry parameters set to zero. The cubic ligand-field calculation provides a very satisfactory reproduction of the experimental data in the 120−296 K temperature regime. A value of $k = 0.7$ was previously inferred for the $[Fe(OH_2)_6]^{2+}$ cation in $Fe(OH_2)_6SiF_6$ on the basis of the low effective magnetic moment at room temperature,[12] but the phenomenon was subsequently suggested as a manifestation of the off-diagonal trigonal field.[13] This is not an issue for the present system owing to the high site symmetry. Nevertheless, we stress that the values of λ and k so obtained should be interpreted with caution. In the Supporting Information, it is shown how dynamic Jahn−Teller coupling simulates the effects of covalency. Magnetic data can be reproduced with higher values of λ and k when dynamic Jahn−Teller coupling is included.

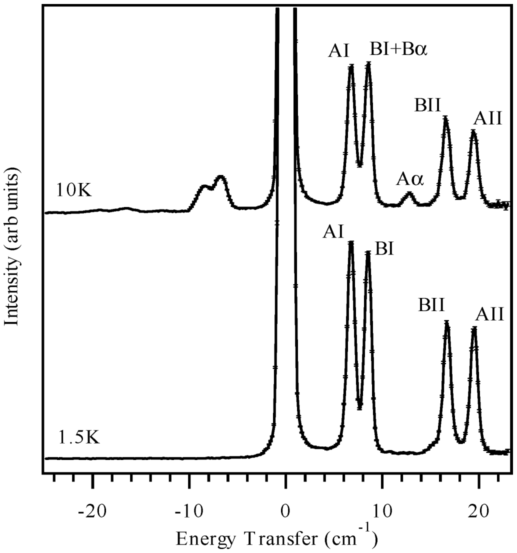

Figure 5. INS spectra of $CsFe(D_2O)_6PO_4$ recorded at 1.5 and 10 K measured on FOCUS with an incident neutron wavelength of 4.75 Å. The transition-labeling scheme follows Figure 6.

4.2. Low-Temperature Phase, 1.5−15 K. Of all the physical techniques applied to characterize the electronic structure of $CsFe(D_2O)_6PO_4$ in the low-temperature phase, INS proved to be the most informative, providing a direct measure of the low-energy excitations in zero field. An interpretation of the low-temperature EPR and Mössbauer spectra was possible only after the INS data were analyzed. Figure 5 shows the INS spectra of $CsFe(D_2O)_6PO_4$ recorded at 1.5 and 10 K, using an incident neutron wavelength of 4.75 Å.

At 1.5 K, the spectrum can be reproduced with a linear background and the superposition of four Gaussian functions, AI, BI, AII, and BII, of equal width, centered at 6.761(3), 8.503(3), 19.480(3), and 16.701(4) cm^{-1}, respectively, on the neutron energy-loss side of the spectrum. At 10 K, the four peaks broaden: a hot peak, Aα, emerges at 12.75(2) cm^{-1}, peaks AI and BI are clearly observable on the neutron energy-gain side, and peaks AII and BII are faintly observable on the energy-gain side. When the temperature increased further, there is the suggestion that the peak positions shift slightly to lower energy. This is commensurate with a pronounced increase in the line widths, and the spectrum is no longer observable at temperatures above 40 K. All the transition intensities decrease with increasing momentum transfer, Q, in accordance with the magnetic form factor,

---

(31) Mabbs, F. E.; Machin, D. J. *Magnetism and Transition Metal Complexes*; Chapman and Hall: New York, 1973.

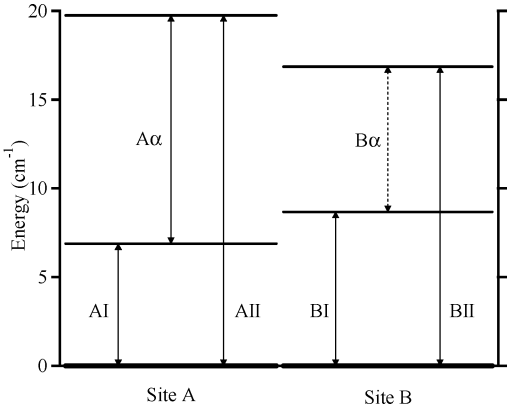

Figure 6. Energy-level diagram depicting the observed INS transitions for the two crystallographically unique $[Fe(OD_2)_6]^{2+}$ complexes, in the low-temperature phase of $CsFe(D_2O)_6PO_4$.

confirming that the transitions are magnetic in origin. Spectra were also obtained with a shorter wavelength of 2.70 Å, affording a larger energy window, but no additional peaks were observed. Spectra obtained on a protonated sample exhibited peaks at similar transition energies.

The INS spectra are not consistent with those expected from a single monomeric Fe(II) complex, no matter how elaborate the Hamiltonian. The data can, however, be readily interpreted assuming that the transitions arise from two crystallographically unique $[Fe(OD_2)_6]^{2+}$ complexes present in a 1:1 ratio. The species are designated A and B, and the peaks labeled in Figure 5 are assigned to the transitions depicted by arrows in Figure 6. The transitions essentially occur between states, which in exact cubic symmetry comprise the three components of the $J = 1$ ground state. The transitions BI and Bα occur at very similar energies and cannot be resolved in the 10 K spectrum. The widths of the INS bands are determined by the instrumental resolution, suggesting a high degree of homogeneity in the low-temperature phase.

In Figure 7, we demonstrate how the experimental spectrum can be reproduced as the sum of two theoretical INS spectra, calculated from different parameter sets, given in the caption. The agreement between the experimental and theoretical values of the transition energies and intensities is striking. Using these parameters, the variation of μ_{eff} with temperature may then be calculated, and this is shown in Figure 4 as the solid line. An excellent reproduction of the experimental data is obtained with these parameters in the 2−15 K temperature regime.

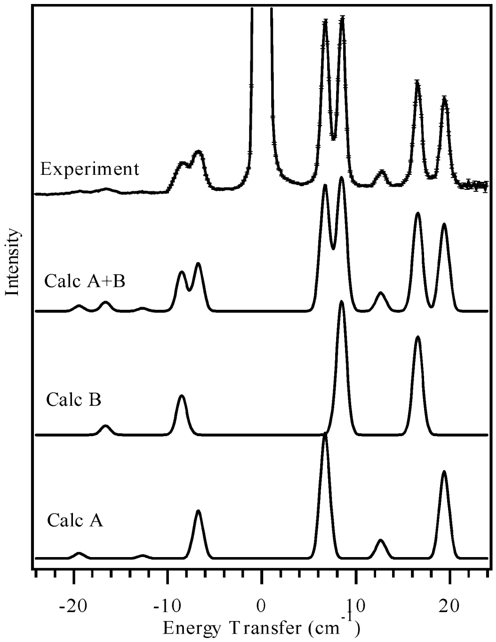

Figure 7. Experimental and calculated INS spectra of $CsFe(D_2O)_6PO_4$ at 10 K. The theoretical spectra were calculated with the following parameters: calcd A $\Delta_{\text{tet}} = 183$ cm^{-1}, $\Delta_{\text{rhom}} = 19$ cm^{-1}; calcd B $\Delta_{\text{tet}} = 181$ cm^{-1}, $\Delta_{\text{rhom}} = 12$ cm^{-1}; both $\lambda = -80$ cm^{-1}, $k = 0.8$. All transitions were folded with a Gaussian line shape with a full-width at half-height of 0.6 cm^{-1}.

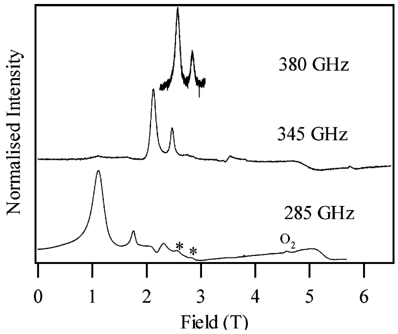

Figure 8. HFEPR spectra of $CsFe(H_2O)_6PO_4$ recorded at 5 K with $\nu \approx$ 285, 345, and 380 GHz. The asterisks on the 285 GHz spectrum denote peaks attributable to contamination from the 380 GHz harmonic. The feature marked O_2 is from an oxygen impurity.

By fitting the eigenvalues of the conventional $S = 2$ spin Hamiltonian

$$\hat{H}_s = D\{\hat{S}_z^{\,2} - (1/3)S(S + 1)\} + E\{\hat{S}_x^{\,2} - \hat{S}_y^{\,2}\} \qquad (2)$$

to the observed INS transition energies, the following spin-Hamiltonian parameters may be derived for the two species: site A $D = 12.02(2)$ cm^{-1}, $E = 2.123(3)$ cm^{-1}; site B $D = 12.15$ cm^{-1}, $E = 1.37$ cm^{-1}. The INS spectra calculated with these parameters were almost identical to the theoretical spectra calculated from the ligand-field Hamiltonian, presented in Figure 7. Alternatively, since the transitions essentially occur between the three components of the $J = 1$ state, perturbed by a small ligand field, the data may be reported in terms of the following parameters pertaining to the $S = 1$ spin Hamiltonian: site A $D = -16.11(2)$ cm^{-1}, $E = 3.375(8)$ cm^{-1}; site B $D = 12.602$ cm^{-1}, $E = 4.099$ cm^{-1}.[32]

EPR spectra recorded on a conventional spectrometer at the X- and Q-band failed to exhibit any resonances attributable to the Fe(II) species, but experiments performed at higher frequencies over a wider field range were more successful. Representative spectra for $CsFe(D_2O)_6PO_4$ are presented in Figure 8. A pair of strong resonances dominate the spectra and shift to higher field with increasing frequency. The resonances observed at 285 GHz broaden and shift ca.

---

(32) Error bars on the parameters could be estimated for species A but not B because three INS transitions could be observed for species A but only two were observed for species B.

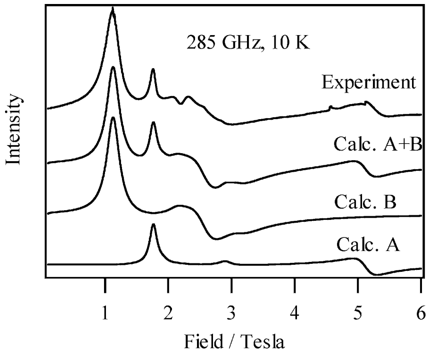

Figure 9. Experimental and theoretical HFEPR spectra of $CsFe(H_2O)_6PO_4$. The theoretical spectra were calculated from the eigenvalues and eigenfunctions of eq 1 using the ligand-field parameters given in Figure 7, assuming that the incident radiation may be deconvoluted into 80% polarized perpendicular and 20% parallel to the applied magnetic field.

500 G to higher field when the temperature is raised to 20 K. Figure 9 shows how the spectrum recorded at 10 K and 285 GHz may be constructed from the sum of two simulations calculated with the ligand-field parameter sets A and B. To obtain a satisfactory reproduction of the band profiles, it was necessary to assume that the incident radiation be composed of 80% polarized perpendicular to the external magnetic field and 20% polarized parallel. Such cross-polarization effects have been noted before[33] and occur as the propagation of the radiation through the sample is not well defined in the HFEPR experiment. All the spectra could be satisfactorily reproduced in this way, providing confidence in the parameter sets derived from the INS and susceptibility data. By fitting the eigenvalues of the $S = 2$ spin Hamiltonian to the eigenvalues of the ligand-field Hamiltonian with the Zeeman term

$$B\beta g\hat{S} \tag{3}$$

added to eq 2, the following $S = 2$ spin-Hamiltonian parameters were derived: site A $D = 12.02(2)$ cm^{-1}, $E = 2.123(3)$ cm^{-1}, $g_x = 2.36$, $g_y = 2.22$, $g_z = 2.52$; site B $D = 12.15$ cm^{-1}, $E = 1.37$ cm^{-1}, $g_x = 2.28$, $g_y = 2.22$, $g_z = 2.52$. EPR spectra calculated with these parameters yielded spectra almost identical to the theoretical spectra presented in Figure 9, calculated from the ligand-field Hamiltonian. The small but significant temperature dependence of the resonance bands, upon increasing temperature from 5 to 20 K, can be reproduced by decreasing the axial ZFS parameter, in accordance with the observed temperature dependence of the INS bands.

The zero-field Mössbauer spectra of $CsFe(H_2O)_6PO_4$ recorded at liquid helium temperatures, shown in Figure 3, exhibit symmetric quadrupole doublets with a large isomer shift of 1.40 mm s^{-1}, typical of high-spin iron(II), coordinated by oxygen-donor (water) ligands.[34]

The electric quadrupole splitting of the Mössbauer spectra is determined by the electric-field gradient, V_{ij}, tensor (efg) at the ^{57}Fe Mössbauer nucleus

$$\Delta E_Q = {}^1\!/_2 eQV_{zz}(1 + \eta^2/3)^{1/2} \tag{4}$$

where the asymmetry parameter, η, is given by the ratio

$$\eta = (V_{xx} - V_{yy})/V_{zz} \tag{5}$$

and Q is the nuclear quadrupole moment, with a value of 0.15 bar.[35] In a ligand-field description of the Fe(II) ion, the valence contribution to the efg is dominant and can be expressed in terms of the orbital operators, L_{ij}[36]

$$V_{ij,\mathrm{val}} = 2/7e\langle r^{-3}\rangle\langle L_{ij}\rangle \tag{6}$$

In the following, we neglect contributions to the efg other than the valence contribution; hence, the quadrupole splitting is given by

$$\Delta E_Q = c^*V_{zz,\mathrm{val}}(1 + \eta_{\mathrm{val}}{}^2/3)^{1/2} \tag{7}$$

In the hypothetical "ionic" limit, where the population of the valence orbitals is not affected by covalency, the proportionality constant would be $c = 2.1$ mm s^{-1}/($^2/_7e\langle r^{-3}\rangle$) for d orbitals with radial parts according to $\langle r^{-3}\rangle = 5a_0{}^{-3}$.

The ground-state $t_{2g}{}^4e_g{}^2$ configuration of the high-spin iron(II) may be considered as a convolution of a hypothetical $t_{2g}{}^3e_g{}^2$ sub-conformation with S-type symmetry and an "extra" electron in a t_{2g} orbital. In this interpretation, the five electrons do not contribute to the efg because of the symmetric charge distribution, but the asymmetry of the extra sixth electron determines the strength of the valence efg, depending on the nature of the orbital state. Furthermore, the expectation values for the efg tensor components, $V_{ii,\mathrm{val}}$, are documented for each of the real d orbitals in octahedral symmetry (Table S4). For an arbitrary orbital state, the components of the efg tensor are obtained as a sum of these (diagonal) expectation values weighted by the corresponding squares of the orbital coefficients.

Tables S5 and S6 give the energies and the squares of the orbital coefficents for the two Fe(II) species, calculated from numerical diagonalization of the $^5T_{2g}$ (O_h) ligand-field Hamiltonian. The orbital energies span a range of ca. 500 cm^{-1}, which implies a substantial variation in the Boltzmann populations of the individual substates in the 4.2−200 K temperature range. The Mössbauer quadrupole splitting was calculated according to eq 7 and averaged over all thermally populated states. The procedure is based on the assumption that the electronic relaxation between the populated substates at any given temperature is fast with respect to the nuclear-quadrupole precession rate and the lifetime ($\cong 10^{-7}$ s) of the ^{57}Fe excited state. The resulting values are shown for both iron species A and B in Figure 10 (solid lines in the middle panel). A reduced factor $c = 1.68$ mm s^{-1}/($^2/_7e\langle r^{-3}\rangle$) was applied to obtain agreement with the experiment at low temperatures. The small reduction in the parameter c from the ionic limit may be attributed primarily to covalency, as well as to lattice contributions. The reduction in c from the

---

(33) Tregenna-Piggott, P. L. W.; Weihe, H. Barra, A.-L. *Inorg. Chem.* **2003**, *42*, 8504−8508.

(34) Greenwood, N. N.; Gibb, T. C. *Mössbauer Spectroscopy*; Chapman and Hall Ltd.: London, 1971.

(35) Ingalls, R. *Phys. Rev.* **1964**, *133*, A787.

(36) Rodriguez, J. H.; Ok, H.; Xia, Y.-M.; Debrunner, P. G.; Hinrichs, B. E.; Meyer, T.; Packard, N. H. *J. Phys. Chem.* **1996**, *100*, 6849.

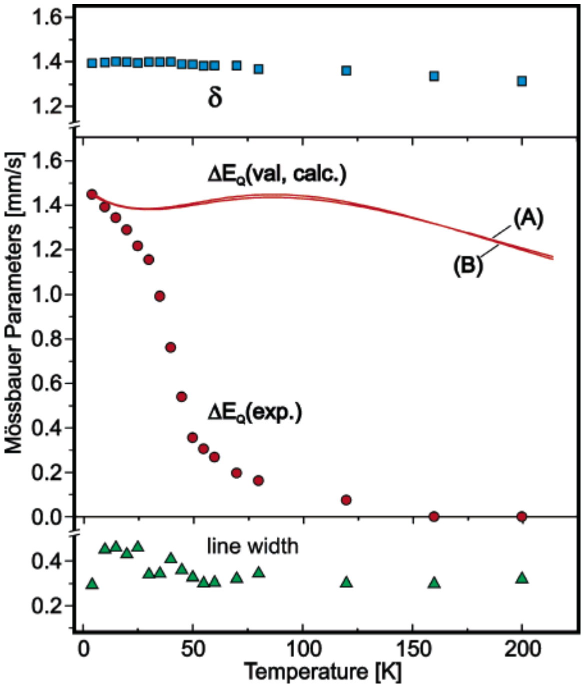

Figure 10. Temperature dependence of the Mössbauer parameters of $CsFe(H_2O)_6PO_4$. The solid lines in the middle panel represent theoretical values for the two iron species, calculated using the ligand-field parameters derived from the analysis of the INS spectra and $c = 1.68$ mm $s^{-1}/(^2/_7 e\langle r^{-3}\rangle)$.

free-ion value is similar to that found for λ and k, and it has a similar physical origin. The differences in the quadrupole splitting for the two iron sites are expected to be substantially less than the Mössbauer line width, and therefore, they cannot be resolved in the experimental spectra.

We note that the z component, $V_{zz,val}$, is the main component of the valence efg for each of the lowest-nine energetically favorable orbital substates. Correspondingly, the thermal average of the valence efg also has a dominating z component in the temperature range of 4.2−200K, and the asymmetry parameters for both species do not exceed $\eta = 0.3 \pm 0.1$ (not shown) for both iron(II) species. The value of η determined was experimentally corroborated from the analysis of the magnetically perturbed Mössbauer spectra and is the same as that reported for the $[Fe(OH_2)_6]^{2+}$ cation in $(NH_4)_2[Fe(H_2O)_6]^{2+}(SO_4)_2$ at 4.2 K.[37] The calculated valence efgs reflect the trend in the experimental values of ΔE_Q up to ca.15 K. Above this temperature, the experimental points are seen to deviate strongly from the theoretical curve.

4.3. Intermediate Temperature Phase, 15−120 K. Above 15 K, the Mössbauer quadrupole splitting of the $CsFe(H_2O)_6PO_4$ salt collapses drastically with increasing temperature, and above ca. 120 K, only a single Mössbauer line at $\delta = 1.3$ mm s^{-1} is observed. Remarkably, the whole transition occurs without substantial line broadening. Figure 10 summarizes the temperature dependence of the Mössbauer parameters that were obtained from the fits of the measured spectra to Lorentzian line doublets. The Mössbauer spectra cannot differentiate between a phase transition or a dynamical process that averages the efg on the time scale of the Mössbauer experiment. The INS time scale is much faster, on the order of 10^{-12} seconds, and the peak positions are noted to shift slightly to lower energy as the temperature is increased, before relaxation effects render the spectrum undetectable. From Figure 4, it is seen that the experimental value of μ_{eff} is consistently greater than the two calculated curves between 15 and 120 K, implying that the high- and low-temperature phases do not coexist in this temperature regime. These spectroscopic and magnetic data are therefore consistent with a gradual increase in the low-symmetry ligand field with decreasing temperature. Q-band EPR spectra of Mn(II) doped $CsFe(H_2O)_6PO_4$ were also recorded as a function of temperature. While the Mn(II) resonances were noted to broaden upon decreasing temperature, the spectra, presented in Supporting Information, provide no further information on the nature of the phase transition.

In an effort to characterize directly the structural changes that occur as a function of temperature, neutron powder diffraction patterns were recorded at 50 and 7 K. The 50 K pattern provided no indication of a phase transition. The data could be refined quite satisfactorily in the $F\bar{4}3m$ space group using the Rietveld method, after peaks attributable to an impurity phase had been subtracted. Refinement details are provided in Table 1 and bond lengths in Table 2. The change in the diffraction pattern upon cooling to 7 K was marginal. The line shapes of the highest-angle reflections were noted to be slightly more asymmetric at 7 K, but neither of the low-temperature patterns gave any obvious indication of a change in space group. Indeed, the 7 K data could once again be refined in the cubic space group, albeit with a significant increase in the goodness-of-fit parameter, χ^2. The unique cell dimension was determined to be 10.02420(9) Å at 50 K, falling to 10.0189(1) Å at 7 K. The contraction in the unit cell is in accordance with expectations. No significant change in the positions of the atomic parameters obtained from the 50 and 7 K refinements could be discerned. Fractional coordinates and thermal parameters are presented in Tables S1 and S2 in the Supporting Information.

The primitive cell for $CsFe(H_2O)_6PO_4$ in space group $F\bar{4}3m$ is rhombohedral with $\alpha = 60°$ and contains just one Fe site. Two unique ordered Fe sites would lead to a doubling of the volume of the primitive cell and the appearance of additional reflections in the powder patterns at 50 and 7 K, but none were observed within the statistics or resolution of our patterns; refinements in a supercell of twice the volume were not attempted. However both the 50 and 7 K refinements did yield larger thermal displacements for the water oxygen atom than for the water deuterium atoms perpendicular to the plane of the water molecule (Table S2, Supporting Information), suggestive of static or dynamic wagging of the water molecule coupled with an O−Fe−O bend or oscillation.

5. Sensitivity of the Ground-State Spin-Hamiltonian Parameters toward Displacements along Normal Coordinates of the $[Fe(OH_2)_6]^{2+}$ Cation

The relationship between the molecular structure and the ground-state spin-Hamiltonian parameters has been of con-

---

(37) Ingalls, R.; Ono, K.; Chandler, L. *Phys. Rev.* **1968**, *172*, 195.

siderable interest of late, as part of the ongoing effort to model the magnetic anisotropy in clusters exhibiting slow relaxation of the magnetic moment.[38,39] In this context it may be of interest that the low-temperature spectroscopic data of $CsFe(H_2O)_6PO_4$ identify two crystallographically distinct $[Fe(OH_2)_6]^{2+}$ cations, each with an appreciable splitting of the $J = 1$ ground state but with a distortion from cubic symmetry too small to be quantified by our crystallographic measurements. In this section, we examine the sensitivity of the energies of the low-lying states of the $[Fe(OH_2)_6]^{2+}$ cation towards small displacements along its normal coordinates. We confine our attention to those displacements that result in a significant splitting of the t_{2g} orbitals, namely, the twisting libration, the $\nu_5(MO_6)$ bend, and the $\nu_2(MO_6)$ stretch, the atomic displacements for which have been depicted previously.[5] These modes transform as *e*, t_2, and *e* respectively in the T_d point group. We take appropriate linear combinations of the components spanning these vibrations to reach points of axial cokernel symmetry. The AOM is chosen as the theoretical framework in which to generate the Hamiltonian, as the expressions derived inter-relate the electronic and molecular structure explicitly.[40]

Twisting Libration. With a basis of clockwise twists of the planes of the water molecule about the metal−oxygen bond vector, the normalized $e(\epsilon)$ libration is defined as

$$Q_\epsilon = {}^1\!/_2(\beta_2 - \beta_3 + \beta_5 - \beta_6) \tag{8}$$

where β_i denotes a unitary increment of the twist angle of the *i*th water molecule. The displacement, ΔQ_ϵ, along this coordinate can then be expressed as

$$\Delta Q_\epsilon = \rho_\epsilon/2(\beta_2 - \beta_3 + \beta_5 - \beta_6) \tag{9}$$

Quantizing along an S_4 axis of a hexa-aqua complex with T_d symmetry, the AOM-Euler angles, $\{\theta, \phi, \psi\}$,[41] of the water molecules are as follows $\{0, 0, \pi/4\}$, $\{\pi/2, 0, -\pi/4 + \rho_\epsilon/2\}$, $\{\pi/2, \pi/2, \pi/4 - \rho_\epsilon/2\}$, $\{\pi/2, \pi, -\pi/4 + \rho_\epsilon/2\}$, $\{\pi/2, 3\pi/2, \pi/4 - \rho_\epsilon/2\}$, and $\{\pi, 0, \pi/4\}$. Using these coordinates, the resulting ligand-field matrix, $\hat{H}_{LF}$, in the real cubic basis has the simple form

$$\left[\begin{array}{llllll} & d_{z^2} & d_{yz} & d_{zx} & d_{xy} & d_{x^2-y^2} \\ d_{z^2} & a & 0 & 0 & 0 & 0 \\ d_{yz} & 0 & c & 0 & 0 & 0 \\ d_{zx} & 0 & 0 & c & 0 & 0 \\ d_{xy} & 0 & 0 & 0 & b & 0 \\ d_{x^2-y^2} & 0 & 0 & 0 & 0 & a \end{array}\right] \tag{10}$$

where $a = 3e_\sigma$, $b = 2(e_{\pi\perp} + e_{\pi\|}) - 2(e_{\pi\|} - e_{\pi\perp}) \sin \rho_\epsilon$, and $c = 2(e_{\pi\perp} + e_{\pi\|}) + (e_{\pi\|} - e_{\pi\perp}) \sin \rho_\epsilon$.

In perfect T_d symmetry, the degeneracy of the $^5T_{2g}$ ground term is lifted by spin−orbit coupling resulting in $J = 1$, $J = 2$, and $J = 3$ manifolds. A small distortion away from T_d symmetry gives rise to a ZFS of the $J = 1$ ground state, which can be described by an effective $S = 1$ spin Hamiltonian, the matrix elements of which are found according to

$$\langle m_s|\hat{H}_{ZFS}|m_s'\rangle = \langle m_j|\hat{H}_{LF}|m_j'\rangle \tag{11}$$

where $|m_s\rangle$ and $|m_s'\rangle$ are states of a fictitious $S = 1$ ground state and $|m_j\rangle$ and $|m_j'\rangle$ are the microstates of the $J = 1$ level. The resulting ZFS matrix is

$$\left[\begin{array}{llll} M_s & |1\rangle & |0\rangle & |-1\rangle \\ \langle 1| & {}^1\!/_{10}(e_{\pi\|} - e_{\pi\perp}) \sin \rho_\epsilon & 0 & 0 \\ \langle 0| & 0 & -{}^1\!/_5(e_{\pi\|} - e_{\pi\perp}) \sin \rho_\epsilon & 0 \\ \langle -1| & 0 & 0 & {}^1\!/_{10}(e_{\pi\|} - e_{\pi\perp}) \sin \rho_\epsilon \end{array}\right] \tag{12}$$

For small distortions where $\rho_\epsilon \ll \pi/2$, $\sin \rho_\epsilon \approx \rho_\epsilon$, and eq 12 simplifies to

$$\left[\begin{array}{llll} & |1\rangle & |0\rangle & |-1\rangle \\ \langle 1| & {}^1\!/_{10}(e_{\pi\|} - e_{\pi\perp})\rho_\epsilon & 0 & 0 \\ \langle 0| & 0 & -{}^1\!/_5(e_{\pi\|} - e_{\pi\perp})\rho_\epsilon & 0 \\ \langle -1| & 0 & 0 & {}^1\!/_{10}(e_{\pi\|} - e_{\pi\perp})\rho_\epsilon \end{array}\right] \tag{13}$$

A comparison of eq 13 to the matrix of an $S = 1$ spin Hamiltonian yields the following expression for the ZFS parameter, *D*

$$D = ({}^3\!/_{10})(e_{\pi\|} - e_{\pi\perp})\rho_\epsilon \tag{14}$$

ν_5 (MO$_6$) Bend. The normalized t_2 (*xz*, *xy*, and *yz*) bending vibrations are defined as

$$\begin{aligned} Q_{xz} &= {}^1\!/_2(\alpha_{15} + \alpha_{24} - \alpha_{12} - \alpha_{45}) \\ Q_{xy} &= {}^1\!/_2(\alpha_{23} + \alpha_{56} - \alpha_{26} - \alpha_{35}) \\ Q_{yz} &= {}^1\!/_2(\alpha_{13} + \alpha_{46} - \alpha_{16} - \alpha_{34}) \end{aligned} \tag{15}$$

where α_{ij} denotes a unitary increment of the O_i−Fe−O_j angle. To simplify our calculations, we construct the linear combination

$$Q_{T_2} = \frac{1}{\sqrt{3}}(Q_{xy} + Q_{xz} + Q_{yz}) \tag{16}$$

corresponding to a simple compression or elongation along the 3-fold axis. The displacement, ΔQ_{T_2}, along this coordinate can then be expressed as

$$\Delta Q_{T_2} = \frac{\rho_{T_2}}{\sqrt{6}}(\alpha_1 + \alpha_2 + \alpha_3 - \alpha_4 - \alpha_5 - \alpha_6) \tag{17}$$

where α_i now denotes a unitary increment of the AOM-Euler angle, θ, for the i^{th} ligand. Quantizing along the 3-fold axis, a displacement along this coordinate results in the following AOM-Euler angles: (1) $\{\gamma + \rho_{T_2}/\sqrt{6}, 0, \pi/2\}$, (2) $\{\gamma + \rho_{T_2}/\sqrt{6}, 2\pi/3, \pi/2\}$, (3) $\{\gamma + \rho_{T_2}/\sqrt{6}, 4\pi/3, \pi/2\}$, (4)$\{\pi - \gamma -$

---

[38] Gatteschi D.; Sorace, L. *J. Solid State Chem.* **2001**, *159*, 253.

[39] Cornia, A.; Sessoli, R.; Sorace, L.; Gatteschi, D.; Barra, A. L.; Daiguebonne, C. *Phys. Rev. Lett.* **2002**, *89*, 257201.

[40] Tregenna-Piggott, P. L. W.; Spichiger, D.; Carver, G.; Frey, B.; Meier, R.; Weihe, H.; Cowan, J. A.; McIntyre, G. J.; Zahn, G.; Barra, A.-L. *Inorg. Chem.* **2004**, *43*, 8049.

[41] Schäffer, C. E. *Struct. Bonding* **1968**, *5*, 68−95.

$\rho_{T_2}/\sqrt{6}, \pi/3, 0\}$, (5)$\{\pi - \gamma - \rho_{T_2}/\sqrt{6}, \pi, 0\}$, and (6)$\{\pi - \gamma - \rho_{T_2}/\sqrt{6}, 5\pi/3, 0\}$, where $\gamma = \arccos(1/\sqrt{3})$.

By analogy to the procedure given above, the following effective $S = 1$ ZFS matrix is constructed

$$\left[\begin{array}{llll} & |1\rangle & |0\rangle & |-1\rangle \\ \langle 1| & \dfrac{(e_{\pi\perp} + e_{\pi\|})\rho_{T_2}}{10\sqrt{3}} & 0 & 0 \\ \langle 0| & 0 & \dfrac{-(e_{\pi\perp} + e_{\pi\|})\rho_{T_2}}{5\sqrt{3}} & 0 \\ \langle -1| & 0 & 0 & \dfrac{(e_{\pi\perp} + e_{\pi\|})\rho_{T_2}}{10\sqrt{3}} \end{array}\right] \tag{18}$$

A comparison of matrix 18 to the matrix of an $S = 1$ spin Hamiltonian yields the following expression for the ZFS parameter, D

$$D = \frac{\sqrt{3}}{10}(e_{\pi\perp} + e_{\pi\|})\rho_{T_2} \tag{19}$$

ν_2(MO$_6$) Stretch. With a basis of Fe−O stretches, the normalized $e(\theta)$ vibration is defined as

$$Q_\theta = \frac{1}{\sqrt{12}}(2r_1 + 2r_4 - r_3 - r_6 - r_2 - r_5) \tag{20}$$

where r_i denotes a unitary increment of the Fe−O$_i$ bond length. The displacement, ΔQ_θ, along the coordinate is then

$$\Delta Q_\theta = \frac{\rho_\theta}{\sqrt{12}}(2r_1 + 2r_4 - r_3 - r_6 - r_2 - r_5) \tag{21}$$

A displacement along this coordinate does not change the AOM angles. Instead the effect is to modify the e_σ and e_π parameters. Assuming a $1/r^5$ and $1/r^6$ dependence of the e_σ and e_π parameters, respectively,[33] we obtain

$$e_{\pi\|,1} = e_{\pi\|,4} = \frac{e_{\pi\|}r_0^{\ 6}}{(r_0 + 2\rho_\theta/\sqrt{12})^6}$$

$$e_{\pi\|,2} = e_{\pi\|,5} = e_{\pi\|,3} = e_{\pi\|,6} = \frac{e_{\pi\|}r_0^{\ 6}}{(r_0 - \rho_\theta/\sqrt{12})^6}$$

$$e_{\pi\perp,1} = e_{\pi\perp,4} = \frac{e_{\pi\perp}r_0^{\ 6}}{(r_0 + 2\rho_\theta/\sqrt{12})^6}$$

$$e_{\pi\perp,2} = e_{\pi\perp,5} = e_{\pi\perp,3} = e_{\pi\perp,6} = \frac{e_{\pi\perp}r_0^{\ 6}}{(r_0 - \rho_\theta/\sqrt{12})^6}$$

$$e_{\sigma,1} = e_{\sigma,4} = \frac{e_\sigma r_0^{\ 5}}{(r_0 + 2\rho_\theta/\sqrt{12})^5}$$

$$e_{\sigma,2} = e_{\sigma,5} = e_{\sigma,3} = e_{\sigma,6} = \frac{e_\sigma r_0^{\ 5}}{(r_0 - \rho_\theta/\sqrt{12})^5} \tag{22}$$

where r_0 is the equilibrium Fe−O bond distance.

The matrix elements of the $S = 1$ spin Hamiltonian are found according to eq 11. Expanding the expressions as a power series in ρ_θ around $\rho_\theta = 0$ and retaining only the first-order terms, the matrix has the form

$$\left[\begin{array}{llll} & |1\rangle & |0\rangle & |-1\rangle \\ \langle 1| & -\dfrac{\sqrt{3}(e_{\pi\perp} + e_{\pi\|})\rho_\theta}{10r} & 0 & 0 \\ \langle 0| & 0 & -\dfrac{\sqrt{3}(e_{\pi\perp} + e_{\pi\|})\rho_\theta}{5r} & 0 \\ \langle -1| & 0 & 0 & -\dfrac{\sqrt{3}(e_{\pi\perp} + e_{\pi\|})\rho_\theta}{10r} \end{array}\right] \tag{23}$$

The axial ZFS parameter is then given by

$$D = -3\sqrt{3}(e_{\pi\perp} + e_{\pi\|})\rho_\theta/10r \tag{24}$$

From eqs 19 and 24, we may conclude immediately that the D parameter is extremely sensitive to displacements along the ν_5(MO$_6$) bending and ν_2(MO$_6$) stretching modes, when the π-bonding is significant. Furthermore, the ZFS can be enhanced significantly when the metal center is coordinated by a nonlinear ligator, since for small distortions along the twisting libration, the magnitude of D is directly proportional to the π anisotropy. This situation pertains to the $[\mathrm{Fe(OH_2)_6}]^{2+}$ complex in $\mathrm{CsFe(H_2O)_6PO_4}$. As an illustration, we consider the distortion along the twisting coordinate required to give a value for D of 13 cm^{-1}, which is on the order of the experimental values ($S = 1$ axial ZFS parameters: site A $D = -16.11(2)$ cm^{-1}; site B $D = 12.602$ cm^{-1}). Given that $e_{\pi\|} - e_{\pi\perp}$ is $\sim$930 cm^{-1} in $[\mathrm{V(OH_2)_6}]^{3+}$ and $10Dq$ $[\mathrm{Fe(OH_2)_6}]^{2+}/10Dq$ $[\mathrm{V(OH_2)_6}]^{3+} \approx 2/3$, the quantity $e_{\pi\|} - e_{\pi\perp}$ for the $[\mathrm{Fe(OH_2)_6}]^{2+}$ complex may be estimated to be $\sim$620 cm^{-1}. Inserting this value into eq 14, with $|D| = 13$ cm^{-1}, we obtain $\rho_\epsilon = 0.070$ rad, equating to a concomitant increment of water molecules 2, 3, 5, and 6 of just 2.0 degrees along the Euler angle, ψ. A large ZFS can result from a relatively small distortion of the $[\mathrm{Fe(OH_2)_6}]^{2+}$ complex, in keeping with our spectroscopic and crystallographic studies of the $\mathrm{CsFe(H_2O)_6PO_4}$ salt.

The $[\mathrm{Fe(OH_2)_6}]^{2+}$ cation has been subject to spectroscopic and magnetochemical studies in a number of crystal systems. Of particular interest are the parameters reported for the perchlorate[7] and hexafluorosilicate[21,42] salts. Telser and coworkers state that the parameters derived should provide a reference point in spin-Hamiltonian parameters for the $[\mathrm{Fe(OH_2)_6}]^{2+}$ cation,[7] which could be understood to mean that the structure of the ferrous complex should, to some extent, reflect the preference of the isolated $[\mathrm{Fe(OH_2)_6}]^{2+}$ cation, since hydrogen-bonding constraints are minimized when aqua ions are crystallized in salts formed from these anions. In both crystal systems, the $[\mathrm{Fe(OH_2)_6}]^{2+}$ cation lies on a site of nominally high symmetry in a trigonal lattice; the site symmetry in the hexafluorosilicate salt is D_{3d}. Nevertheless both the hexafluorosilicate[43] and perchlorate[44] salts exhibit disorder, and the stereochemistry of the aqua ion has not, to

---

(42) Svare, I.; Otnes, K. *Physica B* **1983**, *120*, 159−162.

our knowledge, been determined at temperatures approaching that of liquid He, where magnetic resonance and far-infrared spectra are observed. The $S = 2$ spin-Hamiltonian parameters reported for the $[Fe(OH_2)_6]^{2+}$ cation in these crystal systems are strikingly similar to the values we have derived for the $[Fe(OH_2)_6]^{2+}$ cation in $CsFe(H_2O)_6PO_4$. In the framework of an $S = 2$ spin Hamiltonian, the magnitude of the D parameter reaches a maximum where the axial field and spin−orbit coupling are comparable, and the experimental values for $CsFe(H_2O)_6PO_4$ and the perchlorate and hexafluorosilicate salts are close to the upper limit possible with $\lambda = -80$ cm^{-1}. As we have just shown, a small axial distortion, on the order of the splitting caused by spin−orbit coupling, can result from a relatively small distortion from cubic symmetry. If the complex were to adopt the all-vertical D_{3d} geometry, thus maximizing the splitting of the orbital-triplet ground term, D would be ca. 3.6 cm^{-1}, according to our AOM calculations. This would suggest that the structures of the perchorate and hexafluorosilicate salts are not driven by the stabilization of the ligand-field ground term, in contrast to the hydrates formed from $[Ti(OH_2)_6]^{3+}$,[5,45] $[V(OH_2)_6]^{3+}$,[18,45] and in particular, the $[Ru(OH_2)_6]^{3+}$ cation.[2,46] The extent to which the Jahn−Teller effect dictates the structural chemistry of $CsFe(H_2O)_6PO_4$ is unclear at present. The $[Ni(OH_2)_6]^{2+}$ cation possesses an orbitally nondegenerate ground term, yet our preliminary results[28] indicate that the $CsNi(H_2O)_6PO_4$ salt too exhibits structural instability. On the other hand, EPR measurements on Mn(II) doped $CsMg(H_2O)_6PO_4$ provide no intimation of a phase transition upon cooling in the 2−300 K temperature range. An insight into the preferred mode of water coordination of divalent cations may be afforded by experimental investigations of further members of this family of salts, an occupation that we intend to pursue.

6. Summary and Conclusion

The application of a host of spectroscopic techniques to the $CsFe(H_2O)_6PO_4$ salt has facilitated the rigorous characterization of the electronic structure of the $[Fe(OH_2)_6]^{2+}$ cation in a quasicubic environment. Two crystallographically distinct species exist below 15 K, the magnetic properties of which may be satisfactorily modeled using an elementary ligand-field Hamiltonian operating in the $^5T_{2g}$ ground term. For each species, the splitting of the $J = 1$ ground state is significant and well defined, but the structural distortion from cubic symmetry cannot be identified by the powder diffraction measurements that we have undertaken. The experimental results are in accordance with the AOM analysis, which demonstrates that a large ZFS of the $J = 1$ ground state can result from a relatively small distortion from cubic symmetry. The ZFS parameters of Fe(II) complexes are extremely sensitive to small structural changes when coordinated by π-anisotropic ligands such as water. The AOM is now commonly applied to calculate the ZFS of transition-metal centers, which form an integral part of paramagnetic clusters.[38,39] For such an approach to be meaningfully applied to Fe(II) centers, the mode of bonding of nonlinear ligators must be accurately determined.

Acknowledgment. This work is partly based on experiments performed at the Swiss spallation neutron source SINQ, Paul Scherrer Institute, Villigen, Switzerland. Funding from the Swiss National Science Foundation is gratefully acknowledged.

Supporting Information Available: A large assortment of additional information, including descriptions, equations, figures, and tables, related to this work. This material is available free of charge via the Internet at http://pubs.acs.org.

IC0601889

---

(43) Hamilton, W. C. *Acta Crystallogr.* **1961**, *15*, 353.
(44) Ghost, M.; Siddhartha, R. *Z. Kristallogr.* **1981**, *155*, 129.
(45) Tregenna-Piggott, P. L. W.; Best, S. P. *Inorg. Chem.* **1996**, *35*, 5730.
(46) Dolder, S.; Spichiger, D.; Tregenna-Piggott, P. L. W. *Inorg. Chem.* **2003**, *42*, 1343.